Journal of Neurodevelopmental Cognition

Journal of Neurodevelopmental Cognition 6(3) (2025) 76- 92 10.48308/jncog.2026.242816.1030

ISSN: 2645-565X

http://www.jncog.sbu.ac.ir

Synchronization of Three All-to-All Coupled Hodgkin-Huxley Neurons under an Extremely Low-Frequency Sinusoidal External Electric Field

Mahdi Gholampour*[1], Esmaeil Mahdavi[2], Majid Amirzadeh[3]

[1] *Physics group faculty of basic sciences, Imam Ali University, Tehran, Iran.*

[2] *Department of Physics, Institute for Advanced Studies in Basic Sciences (IASBS), Zanjan, Iran.*

[3] *Physics Group, Faculty of Basic Sciences, Imam Ali University, Tehran, Iran.*

Abstract

Due to the increasing technological exposure to extremely low-frequency (ELF) electromagnetic fields (frequencies less than 300 Hz) and the electrical excitability of neurons, we numerically investigate the impact of an ELF sinusoidal external electric field on the synchronization dynamics of a three-neuron all-to-all Hodgkin–Huxley (HH) network coupled via gap junctions with different output firing rates. Our findings show that the external field can modulate both the degree of synchrony and the firing rate of the network depending on the field frequency, amplitude, and coupling strength, resulting in regimes where synchrony is enhanced, reduced, or remains unchanged. Additionally, the external field can induce explosive synchronization transitions, and in a subset of parameter values (amplitude and frequency of the external electric field), some of these transitions are accompanied by very narrow hysteresis loops. We further demonstrate that the minimum gap-junction conductance required for full network synchrony can decrease, increase, or remain unchanged under external electric field stimulation, highlighting a highly nonlinear and parameter-sensitive interplay between field-driven forcing and intrinsic network dynamics.

Keywords: Hodgkin–Huxley neurons; synchronization; external electric field; hysteresis.

* Corresponding author

Email addresses: nanophys12@gmail.com

Received: June 2025 *Accept: August 2025*

1. Introduction

Human exposure to electromagnetic fields, which consist of time-varying electric and magnetic fields, has become unavoidable with the rapid advancement of modern technologies (*Kama et al., 2019*). These fields are now pervasive in daily life, arising from sources such as power transmission lines, household appliances, and a growing range of medical and communication technologies. Although studies have suggested a possible link between electromagnetic fields exposure and the development of many neuronal diseases (*kama et al.*) electromagnetic brain stimulation has, conversely, emerged as an effective tool in neuroscience and clinical practice (*Peterchev et al., 2012*). Deep brain stimulation (DBS), which works through targeted electrical stimulation, is recognized as an effective therapeutic intervention for Parkinson's disease and other neurological disorders, such as dystonia, by modulating abnormal neural activity within specific brain regions (*Rubin & Terman, 2004; Hariz & Blomstedt, 2022; Krack et al., 2003; Toda et al., 2004; Hale et al., 2020*). Transcranial magnetic stimulation (TMS) has also been established as an effective, noninvasive technique for the treatment of neurological and psychiatric disorders such as epilepsy and depression (*wagner et al., 2007; Walsh & Coway, 2000; Walton et al., 2021; Soma et al., 2022*). Furthermore, related modalities—including repetitive transcranial magnetic stimulation (rTMS) (*Soma et al.; Klimesch et al., 2003*), low-field magnetic stimulation (LFMS) (*Mellon et al., 2024*), and pulsed magnetic field (PMF) therapy (*Mert, 2017*)—have demonstrated efficacy in alleviating symptoms across a range of neurological conditions.

Because neurons are electrically excitable cells, they are inherently sensitive to external electric and magnetic fields. Numerous studies have demonstrated that such fields, as well as other external stimuli, can influence neuronal dynamics and alter firing patterns (*Roth & Basser, 1990; Lv & Ma, 2016; Gianni et al., 2006; Li et al., 2016; Doi et al., 2001; Gu et al., 2003; Wu-Yin et al., 2004*). While electromagnetic fields are therapeutically applied to modulate neural activity and treat a variety of neurological disorders, inappropriate or uncontrolled disturbances in neuronal excitability can lead to abnormal firing patterns and, consequently, to pathological conditions (*Smeal et al., 2010*). These findings highlight the critical importance of understanding the complex interactions between electromagnetic fields and the nervous system.

Mathematical modeling provides a powerful framework for describing the generation and modulation of action potentials and for investigating the interactions between neurons and external stimuli. Among the available computational approaches, the HH model—a system of four-dimensional nonlinear differential equations—remains a fundamental one due to its high biophysical fidelity (*Hodgkin & Huxley, 1952; Izhikevich, 2004*). This model, along with the simpler Morris–Lecar (ML) model (*Morris & Lecar, 1981; Rinzel & Ermentrout, 1998*), is widely used to explore the effects of external perturbations, such as time-dependent electric and magnetic fields, on neuronal dynamics. Of particular interest are ELF fields, typically below 100 Hz, which coincide with environmental exposures and the frequency range of biological neural oscillations, making their study especially relevant for understanding neuronal responses to external electromagnetic stimuli (*Saby & Marshall, 2012; Tian et al., 2023).*

Previous studies, based on the HH and ML models, have shown that ELF electric fields can significantly influence neuronal activity. Most of these investigations have been performed on quiescent (silent) neurons. Depending on the amplitude and frequency of the applied electric field, neurons can exhibit a range of dynamical behaviors, including subthreshold oscillations, various types of p: q mode-locking (where p spikes occur per q cycles of stimulation), and chaotic activity (*Che et al., 2009; Han et al., 2009; Yi et al., 2012; Nkomidio et al., 2022; Yi et al., 2014*). Furthermore, increasing the external DC current in the presence of a sinusoidal ELF electric field induces additional dynamical regimes, including quasi-periodic oscillations (*Gholampour et al., 2026*). Examination of the ISI diagram, in which the frequency of the external electric field acts as a bifurcation parameter, shows a rich and complex bifurcation structure. Variations in the frequency of the external electric field can induce transitions between distinct dynamical regimes (*Che et al., 2009; Han et al., 2009; Yi et al., 2012; Nkomidio et al., 2022; Gholampour et al., 2026*). Analysis of bifurcations induced by an external electric field, using the field's voltage as a bifurcation parameter, has identified critical equilibrium points (*Wang et al., 2003; Jiang et al., 2005*). Investigation of synchronization in two unidirectionally coupled HH neurons (*Wang et al., 2009; Che et al., 2009; Wang et al., 2007*) and two weakly coupled ML neurons, interconnected by a gap junction (*Nkomidio et al. 2022*), demonstrates that these neurons can achieve synchronization under the influence of an ELF external electric field.

In active HH neurons, whether in spiking, bursting, or bistable states, exposure to ELF magnetic fields can modulate neuronal firing, producing either increases or decreases in spike frequency and inducing diverse dynamical behaviors. Even in the bistable state, external stimulation may suppress firing entirely, while neurons in the bursting state exhibit the least sensitivity to temporal variations in their firing patterns (*Yang et al., 2022*). Similarly, studies of active ML neurons have shown distinct dynamical responses to ELF magnetic field stimulation across spiking and firing regimes (*Yi et al, 2014*).

Given the limited number of studies on synchronization in neuronal populations under ELF external electric field stimulation, and considering that neuronal synchrony plays a crucial role in information transmission (*Buzsaki & Draguhn, 2004*), the present study investigates the synchrony of three fully connected HH neurons coupled by gap junctions in the presence of a sinusoidal ELF electric field.

The paper is organized as follows: Section 2 introduces the mathematical model used to analyze neuronal dynamics under the influence of an external sinusoidal electric field. Section 3 presents and discusses the numerical results, and Section 4 concludes the paper with a summary of the main findings.

2. Method

We have employed the HH model in our simulations, which describes the evolution of the neuronal membrane potential through the following four differential equations (*Hodgkin & Huxley, 1952*):

$$C\frac{dV_i}{dt} = I_{\mathrm{inj},i} + I_{\mathrm{gap},i} - \bar{g}_{\mathrm{Na}} m_i^3 h_i (V_i - V_{\mathrm{Na}}) - \bar{g}_{\mathrm{K}} n_i^4 (V_i - V_{\mathrm{K}}) - \bar{g}_{\mathrm{L}} (V_i - V_{\mathrm{L}}), \qquad (1)$$

$$\frac{dm_i}{dt} = \alpha_m(V_i)(1 - m_i) - \beta_m(V_i)m_i, \quad (2)$$
$$\frac{dh_i}{dt} = \alpha_h(V_i)(1 - h_i) - \beta_h(V_i)h_i, \quad (3)$$
$$\frac{dn_i}{dt} = \alpha_n(V_i)(1 - n_i) - \beta_n(V_i)n_i. \quad (4)$$

where i, C, V, and t are the nouron index, the capacitance per serface unit, the membrane potential, and time, respectively. $I_{\mathrm{inj},i}$ is a constant injected intracellular current for neuron i, and $I_{\mathrm{gap},i} = g_{\mathrm{gap}} \sum_{j=1,j\neq i}^{N} (V_j - V_i)$ represents the total gap-junction current into neuron i. Here, g_{gap} is the gap-junction conductance that controls the strength of electrical coupling between neurons in a network of size N. The parameters $\bar{g}_{\mathrm{Na}}$, $\bar{g}_{\mathrm{K}}$, and $\bar{g}_{\mathrm{L}}$ are the maximal values of the conductances for the sodium, potassium, and leakage currents, respectively. V_{Na}, V_{K}, and V_{L} are the corresponding respective reversal potentials. The parameter values for Equation (1) are listed in Table 1.

The variables m, h, and n are the activation variable of the sodium current, the inactivation variable of the sodium current, and the activation variable of the potassium current, respectively. The corresponding α and β rate functions are given by the following equations:

$$\begin{aligned}
&\alpha_m(V) = 0.1(V + 45)/\left(1 - \exp\left(-0.1(V + 45)\right)\right),\\
&\alpha_h(V) = 0.07\exp\left(-0.05(V + 70)\right),\\
&\alpha_n(V) = 0.01(V + 60)/\left(1 - \exp\left(-0.1(V + 60)\right)\right),\\
&\beta_m(V) = 4\exp(-(V + 70)/18),\\
&\beta_h(V) = 1/\left(1 + \exp\left(-0.1(V + 40)\right)\right),\\
&\beta_n(V) = 0.125\exp(-(V + 70)/80).
\end{aligned} \quad (5)$$

We consider a time-dependent sinusoidal external electric field in the ELF range, given by:

$$E = E_{\mathrm{EF}} \sin(2\pi f_{\mathrm{EF}} t), \quad (6)$$

where E_{EF} is the amplitude and f_{EF} is the frequency of the external electric field. Applying this field to the brain induces charge transfer within neural tissue, generating a current flow mainly in the extracellular environment (*Attwell, 2003*). Therefore, the external electric field produces a membrane depolarization ΔV, whose dynamics are described by the following equation (*Bédard et al., 2006*):

$$\frac{d\Delta V}{dt} + \frac{\Delta V}{\tau} = \frac{\lambda}{\tau} E, \quad (7)$$

Table 1: *The parameter values of Equation (1).*

symbol	C	V_{Na}	V_K	V_L	$\bar{g}_{\mathrm{Na}}$	$\bar{g}_K$	$\bar{g}_L$
value	$1\ \frac{\mu\mathrm{F}}{\mathrm{cm}^2}$	$45\ \mathrm{mV}$	$-82\ \mathrm{mV}$	$-59\ \mathrm{mV}$	$120\ \frac{\mathrm{mS}}{\mathrm{cm}^2}$	$36\ \frac{\mathrm{mS}}{\mathrm{cm}^2}$	$0.3\ \frac{\mathrm{mS}}{\mathrm{cm}^2}$

where λ is the polarization length, and τ is the Maxwell–Wagner time constant. The solution of Equation (7) is given by:

$$\Delta V = V_{\mathrm{EF}} \frac{\sin(\omega t) - \omega\tau \cos(\omega t)}{1 + (\omega\tau)^2}, \tag{8}$$

where $V_{\mathrm{EF}} = \lambda E_{\mathrm{EF}}$ and $\omega = 2\pi f_{\mathrm{EF}}$. Since our study focuses on ELF and the Maxwell–Wagner time constant τ is very small (*Bédard et al., 2006*}, Equation (7) can be approximated as:

$$\Delta V = V_{\mathrm{EF}} \sin(\omega t). \tag{9}$$

The effect of the sinusoidal ELF field is introduced as an additive perturbation of magnitude ΔV to the membrane potential in Equation (1), while Equations (2) to (4) remain unchanged. The modified equations are therefore written as:

$$\begin{aligned} C\frac{dV_i}{dt} = {} & I_{\mathrm{ind},i} + I_{\mathrm{inj},i} + I_{\mathrm{gap},i} - \bar{g}_{\mathrm{Na}} m_i^3 h_i (V_i + \Delta V - V_{\mathrm{Na}}) \\ & - \bar{g}_{\mathrm{K}} n_i^4 (V_i + \Delta V - V_{\mathrm{K}}) - \bar{g}_{\mathrm{L}} (V_i + \Delta V - V_{\mathrm{L}}), \end{aligned} \tag{10}$$

$$\frac{dx_i}{dt} = x_m(V_i)(1 - x_i) - \beta_m(V_i) x_i, \quad x = m, h, n. \tag{11}$$

This perturbation produces an induced current $I_{\mathrm{ind}} = -C\ d\Delta V/dt$ in the membrane capacitance, and shifts the reversal potentials of the sodium, potassium, and leakage currents by ΔV due to the externally applied electric field. It is worth noting that the current generated by the gap junction remains unchanged because the same perturbation is induced in all neurons.

To quantify the degree of synchronization, we use the synchronous voltage measure M, defined as:

$$M = \frac{\sqrt{\langle V_g^2(t)\rangle_t - \langle V_g(t)\rangle_t^2}}{\frac{1}{N}\sum_{i=1}^{n} \sqrt{\langle V_i^2(t)\rangle_t - \langle V_i(t)\rangle_t^2}}, \tag{12}$$

where $V_g(t) = \frac{1}{N}\sum_{i=1}^{N} V_i(t)$ is the global average membrane potential. The measure satisfies $0 \le M \le 1$, where $M = 0$ indicates a completely asynchronous state and $M = 1$ corresponds to full synchrony state.

3. Results and Discussion

We coupled three active neurons with different intrinsic firing frequencies by injecting distinct constant currents into each neuron. Specifically, we set the injected currents to $I_{\mathrm{inj},1} = 6.15\ \mu\mathrm{A/cm^2}$, $I_{\mathrm{inj},2} = 10.5\ \mu\mathrm{A/cm^2}$, and $I_{\mathrm{inj},3} = 22.4\ \mu\mathrm{A/cm^2}$. In the absence of coupling and without an external electric field, the corresponding output firing frequencies are $f_{\mathrm{out},1} = 51.11$ Hz, $f_{\mathrm{out},1} = 69.83$ Hz, and $f_{\mathrm{out},1} = 89.89$ Hz. For $I_{\mathrm{inj}} > 9.6\ \mu\mathrm{A/cm^2}$, the neuron remains in an active spiking state, whereas for $I_{\mathrm{inj}} \in (6.1, 9.6]\ \mu\mathrm{A/cm^2}$ the HH model exhibits a bistable regime in which both active and silent states coexist (*Börgers, 2017*). We therefore selected the initial conditions such that all neurons were in the active state in the uncoupled and field-free configuration.

We use the fourth-order Runge-Kutta method to numerically integrate Equations (10) and (11) with a time step of $dt = 0.01$ ms. The total simulation time is chosen as

$t = \max\{40000, 40000/f_{\mathrm{EF}}(\mathrm{Hz})\}$ ms, where $40000/f_{\mathrm{EF}}(\mathrm{Hz})$ corresponds to 40 cycles of the external sinusoidal electric field, expressed in milliseconds.

Figure 1 shows the voltage dynamics of three HH neurons in the absence of an external electric field for different values of the gap-junction conductance, $g_{\mathrm{gap}} = 0, 0.13, 0.41, 1.03\ \mathrm{mS/cm^2}$. The blue, red, and green curves correspond to the first, second, and third neurons, respectively. When no coupling is present (Figure 1a), each neuron oscillates at its own intrinsic frequency, resulting in a synchrony measure of $M = 0.58$. As g_{gap} increases, the membrane potentials of the neurons progressively converge, leading to a higher degree of synchrony. At $g_{\mathrm{gap}} = 1.03\ \mathrm{mS/cm^2}$, the neurons exhibit near-perfect synchrony with $M = 0.99$.

By introducing a weak sinusoidal external electric field with $V_{\mathrm{EF}} = 2\ \mathrm{mV}$, both the firing frequencies and the degree of synchronization of the neurons are changed. Figure 2 displays the voltage dynamics of the three HH neurons in the presence of an external electric field with frequency $f_{\mathrm{EF}} = 70.3\ \mathrm{Hz}$ (the mean of the three intrinsic neuronal frequencies) for different values of the gap-junction conductance, $g_{\mathrm{gap}} = 0, 0.05, 0.31, 0.9\ \mathrm{mS/cm^2}$. In each panel, the black dashed curve represents the external electric field.

When the neurons are uncoupled ($g_{\mathrm{gap}} = 0$), the external field alone is sufficient to entrain their firing frequencies to its own, although the overall synchrony is reduced compared to the field-free case ($M = 0.48$). For nonzero coupling strengths, the neurons lock to the frequency of the external field, while the gap junctions primarily align the timing and shape of spikes, thereby enhancing population synchrony. In Figures 2b, 2c, and 2d, the order parameter takes the same values as in the corresponding panels of Figure 1, indicating that near-complete synchrony is achieved at considerably smaller coupling strengths. Thus, the external electric field not only shifts the neuronal firing frequency but also promotes full synchronization at reduced gap-junction conductance, reaching $M = 0.99$ at $g_{\mathrm{gap}} = 0.9\ \mathrm{mS/cm^2}$ in Figure 2d.

Figure 1: *Membrane potential dynamics of three all-to-all coupled HH neurons in the absence of an external electric field for different values of the gap-junction conductance: (a) $g_{gap} = 0\ mS/cm^2$, (b) $g_{gap} = 0.13\ mS/cm^2$, (c) $g_{gap} = 0.41\ mS/cm^2$, and (d) $g_{gap} = 1.03\ mS/cm^2$. The blue, red, and green lines correspond to the first, second, and third neurons, respectively, with injected currents $I_{inj,1} = 6.15\ \mu A/cm^2$, $I_{inj,2} = 10.5\ \mu A/cm^2$, and $I_{inj,3} = 22.4\ \mu A/cm^2$.*

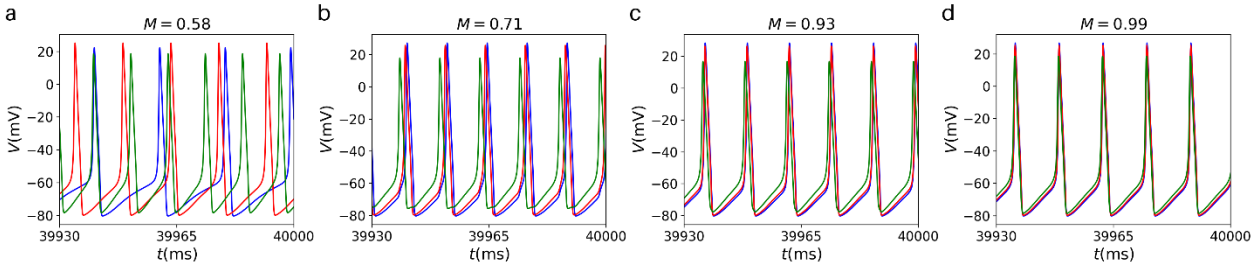

Figure 2: *Membrane potential dynamics of three all-to-all coupled HH neurons under an external sinusoidal electric field with amplitude $V_{EF} = 2\ mV$ and frequency $f_{EF} = 70.3\ Hz$ (black dashed line), for different values of the gap-junction conductance: (a) $g_{gap} = 0\ mS/cm^2$, (b) $g_{gap} = 0.05\ mS/cm^2$, (c) $g_{gap} = 0.31\ mS/cm^2$, and (d) $g_{gap} = 0.9\ mS/cm^2$. The blue, red, and green lines correspond to the first, second, and third neurons, respectively, with injected currents $I_{inj,1} = 6.15\ \mu A/cm^2$, $I_{inj,2} = 10.5\ \mu A/cm^2$, and $I_{inj,3} = 22.4\ \mu A/cm^2$.*

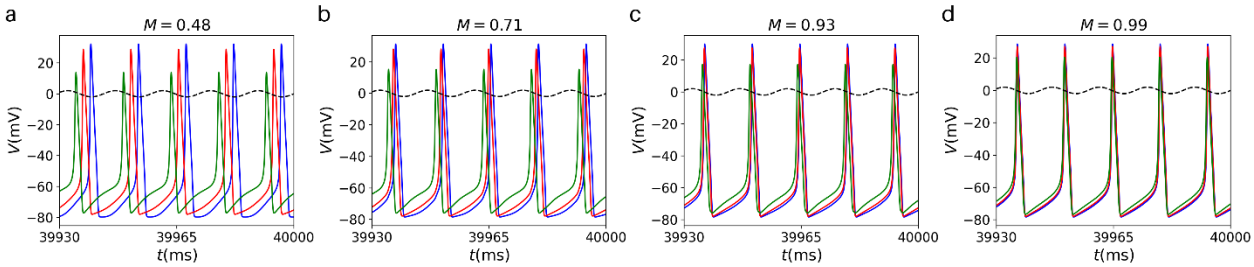

Since both the frequency and amplitude of the external electric field affect neuronal synchrony and firing rate, Figure 3 presents the voltage synchrony measure M (subpanel (i)) and the average firing rate $\langle f_{\text{out}} \rangle$ (subpanel (ii)) versus gap-junction conductance for several field frequencies and amplitudes. Panels a-d correspond to $f_{\text{EF}} = 0.1, 10, 70.3, 150$ Hz.

For low field frequencies (Figures 3a and 3b), synchronization varies irregularly for $g_{\text{gap}} \leq 0.11\ \text{mS/cm}^2$, but increases monotonically for larger coupling strengths. When the field frequency is much lower than the intrinsic neuronal frequencies, increasing the amplitude of the external field allows the network to reach full synchrony at smaller values of g_{gap}. Thus, in the strong-coupling regime, a larger field amplitude enhances the degree of synchronization.

Figure 3: *(i) Voltage synchrony measure M and (ii) average firing rate $\langle f_{out} \rangle$ versus the gap-junction conductance for three all-to-all coupled HH neurons, shown for different external electric field amplitudes and four field frequencies: (a) $f_{EF} = 0.1\ Hz$, (b) $f_{EF} = 10\ Hz$, (c) $f_{EF} = 70.3\ Hz$, and (d) $f_{EF} = 150\ Hz$. The injected currents are $I_{inj,1} = 6.15\ \mu A/cm^2$, $I_{inj,2} = 10.5\ \mu A/cm^2$, and $I_{inj,3} = 22.4\ \mu A/cm^2$.*

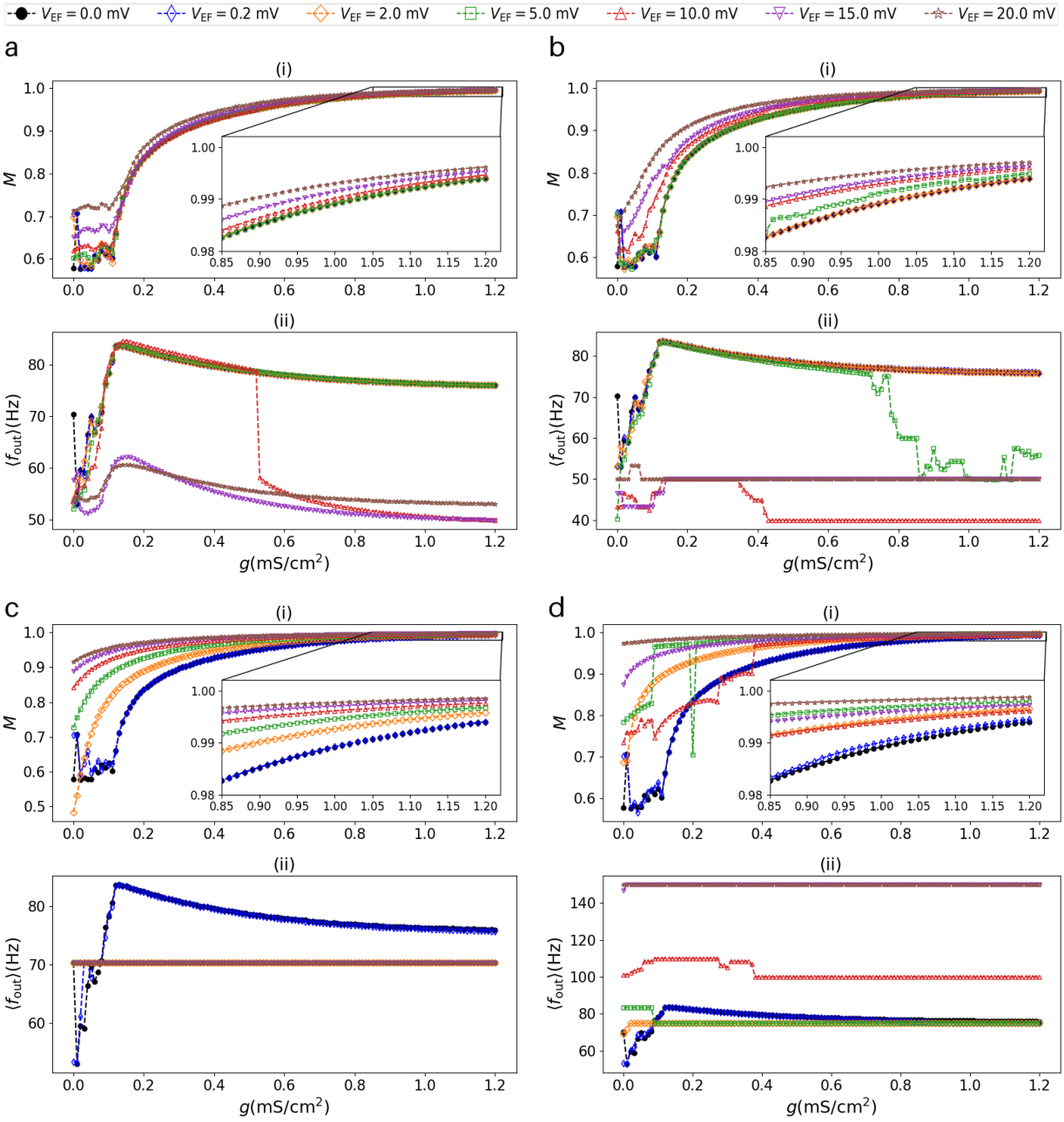

The output firing rate exhibits more complex behavior than the synchronization measure, depending strongly on the amplitude and frequency of the external electric field. In Figure 3a, for small amplitudes ($V_{\mathrm{EF}} = 0, 0.2, 2, 5\ \mathrm{mV}$), the average firing rate first increases and then

decreases as g_{gap} approaches $0.13\ \mathrm{mS/cm^2}$. For larger amplitudes ($V_{\mathrm{EF}} = 15, 20\ \mathrm{mV}$), it decreases smoothly at first, then increases, and begins to decline again for $g_{\mathrm{gap}} \geq 0.16\ \mathrm{mS/cm^2}$, indicating two distinct average firing rate regimes. For $V_{\mathrm{EF}} = 10\ \mathrm{mV}$, the behavior is similar to the small-amplitude case, but a clear transition between the two regimes appears around $g_{\mathrm{gap}} = 0.52\ \mathrm{mS/cm^2}$.

At a higher field frequency $f_{\mathrm{EF}} = 10\ \mathrm{Hz}$ (Figure 3b), amplitudes $V_{\mathrm{EF}} = 10, 15, 20\ \mathrm{mV}$ show multiple frequency transitions as g_{gap} increases, eventually settling to a constant firing rate beyond a threshold value of g_{gap}. In this region, synchronization grows steadily, indicating that the external field enforces a stable firing frequency while coupling aligns spike timing. For $V_{\mathrm{EF}} = 5\ \mathrm{mV}$, the main difference from Figure 3a is that the average firing rate begins to switch irregularly among discrete values once g_{gap} exceeds $0.72\ \mathrm{mS/cm^2}$.

When the external field frequency matches the average intrinsic neuronal frequency ($f_{\mathrm{EF}} = 70.3\ \mathrm{Hz}$ in Panel d), the low-amplitude cases ($V_{\mathrm{EF}} = 0, 0.2\ \mathrm{mV}$) behave similarly to Figure 3a and Figure 3b. For larger amplitudes, the neurons become entrained to the field even without coupling, and increasing g_{gap} strengthens synchrony. In particular, a strong field ($V_{\mathrm{EF}} = 20\ \mathrm{mV}$) produces high synchrony ($M > 0.9$) even at $g_{\mathrm{gap}} = 0$.

At a higher field frequency ($f_{\mathrm{EF}} = 150\ \mathrm{Hz}$), the $V_{\mathrm{EF}} = 5\ \mathrm{mV}$ and $10\ \mathrm{mV}$ cases show additional average firing rate transitions as g_{gap} increases before settling into behavior similar to the other panels. In this regime, $V_{\mathrm{EF}} = 5\ \mathrm{mV}$ reaches full synchrony earlier than all amplitudes except $V_{\mathrm{EF}} = 20\ \mathrm{mV}$. These observations highlight the complex, nonlinear interplay between the external electric field and the intrinsic neuronal dynamics in the presence of gap-junction coupling.

To investigate whether the external electric field induces hysteresis in the network, we computed the synchrony measure and average firing rate for $f_{\mathrm{EF}} = 150\ \mathrm{Hz}$ across different V_{EF} values in forward (blue hollow diamonds) and backward (red solid circles) directions, shown in Figure 4. Panels a-d correspond to $V_{\mathrm{EF}} = 0, 5, 10, 15\ \mathrm{mV}$, respectively, with subpanels (i) and (ii) displaying M and $\langle f_{\mathrm{out}} \rangle$. The results indicate that the external field rarely generates a hysteresis loop associated with explosive phase transitions, for a narrow gap-junction width of $g_{\mathrm{gap}} = 0.01\ \mathrm{mS/cm^2}$ (panel b). Furthermore, not all explosive transitions necessarily produce hysteresis (panel c).

To systematically characterize how the amplitude and frequency of the external electric field influence network synchronization and average firing rate, we computed both quantities across the V_{EF}-f_{EF} plane for several values of the gap-junction conductance. The results are shown in Figure 5. Panels a-f correspond to $g_{\mathrm{gap}} = 0, 0.04, 0.1, 0.2, 0.5, 0.9\ \mathrm{mS/cm^2}$, respectively. Each panel contains two subpanels: (i) the synchronization measure M and (ii) the average firing rate $\langle f_{\mathrm{out}} \rangle$, each represented by a color scale.

Figure 4: *(i) Voltage synchrony measure M and (ii) average firing rate $\langle f_{\text{out}} \rangle$ versus the gap-junction conductance for three all-to-all coupled HH neurons in the forward and backward directions, shown for $f_{\text{EF}} = 150$ Hz and different external electric field amplitudes: (a) $V_{\text{EF}} = 0$, (b) $V_{\text{EF}} = 5$ mV, (c) $V_{\text{EF}} = 10$ mV, and (d) $V_{\text{EF}} = 15$ mV. The injected currents are $I_{\text{inj},1} = 6.15\ \mu\text{A/cm}^2$, $I_{\text{inj},2} = 10.5\ \mu\text{A/cm}^2$, and $I_{\text{inj},3} = 22.4\ \mu\text{A/cm}^2$.*

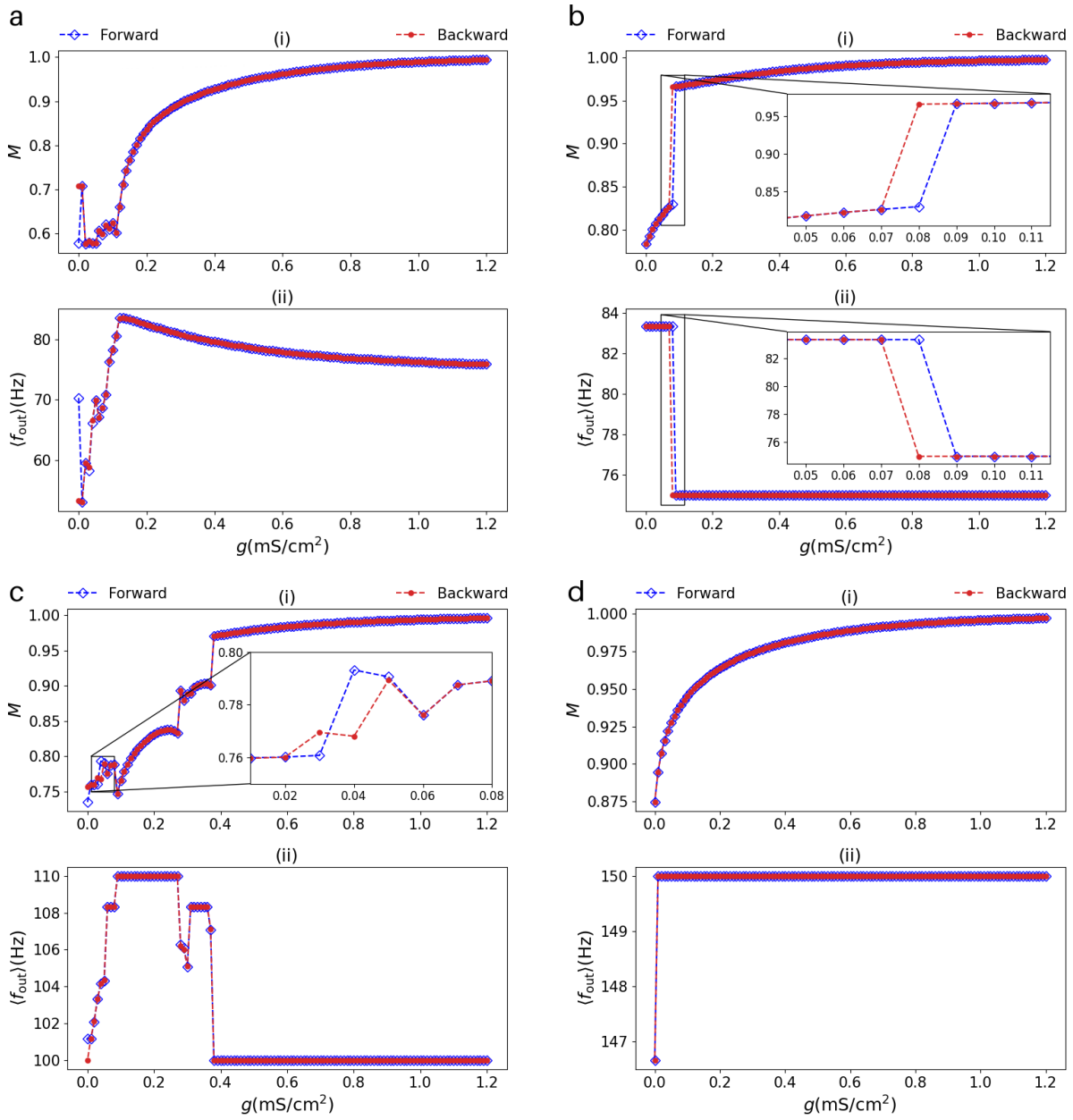

Results show that the external electric field alone can both enhance and suppress network synchrony and average firing rate. In Figure 5a ($g_{\text{gap}} = 0$), where no electrical coupling is present, the minimum synchrony occurs at $V_{\text{EF}} = 1.8$ mV and $f_{\text{EF}} = 71.5$ Hz, yielding $M = 0.44$, while the maximum appears at $V_{\text{EF}} = 20$ mV and $f_{\text{EF}} = 150$ Hz, where $M = 0.97$.

Figure 5: *(i) Voltage synchrony measure M and (ii) average firing rate $\langle f_{\mathrm{out}} \rangle$ (measured in* Hz*) in the V_{EF}-f_{EF} plane for three all-to-all coupled HH neurons across different values of the gap-junction conductance: (a) $g_{\mathrm{gap}} = 0$, (b) $g_{\mathrm{gap}} = 0.04\ \mathrm{mS/cm^2}$, (c) $g_{\mathrm{gap}} = 0.1\ \mathrm{mS/cm^2}$, (d) $g_{\mathrm{gap}} = 0.2\ \mathrm{mS/cm^2}$, (e) $g_{\mathrm{gap}} = 0.5\ \mathrm{mS/cm^2}$, and (f) $g_{\mathrm{gap}} = 0.9\ \mathrm{mS/cm^2}$. The injected currents are $I_{\mathrm{inj},1} = 6.15\ \mu\mathrm{A/cm^2}$, $I_{\mathrm{inj},2} = 10.5\ \mu\mathrm{A/cm^2}$, and $I_{\mathrm{inj},3} = 22.4\ \mu\mathrm{A/cm^2}$.*

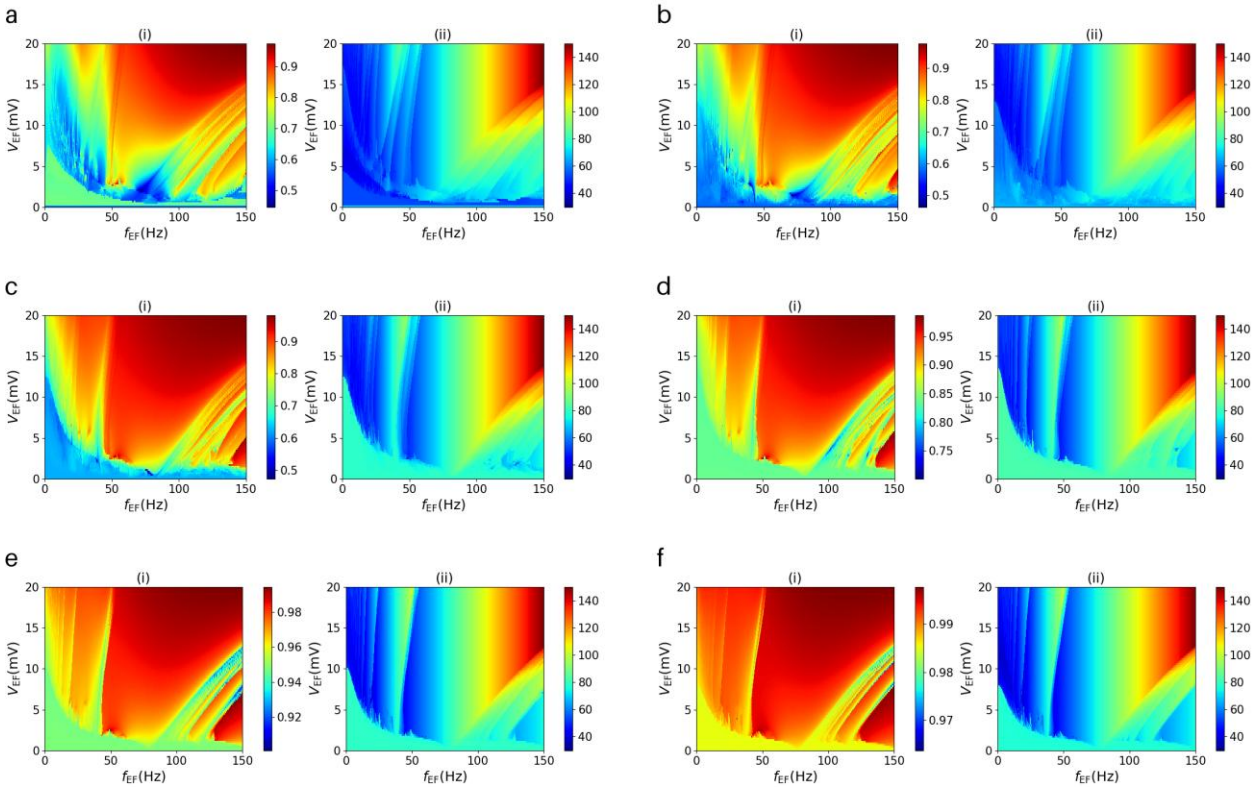

The dependence of the network synchronization on the amplitude and frequency of the external electric field does not follow a regular or monotonic pattern. Nevertheless, the highest synchronization values generally occur at the largest field amplitudes and frequencies examined in this study. In contrast, the locations of the minimum synchronization values vary with the gap-junction conductance. For panels a-c, the minimum synchrony appears within intermediate field frequencies and at low amplitudes ($V_{\mathrm{EF}} < 2\ \mathrm{mV}$). For the remaining panels, the lowest synchronization occurs at high frequencies ($f_{\mathrm{EF}} > 135\ \mathrm{Hz}$) and medium-to-low amplitudes ($V_{\mathrm{EF}} \leq 10\ \mathrm{mV}$).

These findings demonstrate that increasing the amplitude of the external electric field does not necessarily enhance network synchrony; in some regimes, it can even reduce it. Overall, the network's response is highly nonlinear, reflecting the complex interplay among gap-junction coupling, intrinsic neuronal dynamics, and the external electric field.

The maximum average firing rate occurs at $f_{\mathrm{EF}} = 150\ \mathrm{Hz}$ for all values of the gap-junction conductance, indicating that the neuronal firing frequency becomes fully entrained to the

external field at this frequency. The gap-junction conductance also modulates the range of field amplitudes that produce this maximal firing rate: stronger electrical coupling allows larger ranges of V_{EF} to induce peak activity. For example, when $g_{\mathrm{gap}} = 0$ and $g_{\mathrm{gap}} = 0.9\ \mathrm{mS/cm^2}$, the amplitudes leading to the maximum average firing rate lie within $V_{\mathrm{EF}} \in [15.2, 20]\ \mathrm{mV}$ and $V_{\mathrm{EF}} \in [12.8, 20]\ \mathrm{mV}$, respectively.

The minimum firing rate depends on the value of g_{gap}, but across all coupling strengths it consistently occurs within the region $f_{\mathrm{EF}} < 29.4\ \mathrm{Hz}$ and $V_{\mathrm{EF}} < 11.5\ \mathrm{mV}$. As an example, for $g_{\mathrm{gap}} = 0.9\ \mathrm{mS/cm^2}$, the minimum average firing rate appears at $f_{\mathrm{EF}} = 29.3\ \mathrm{Hz}$ and $V_{\mathrm{EF}} = 11.4\ \mathrm{mV}$, corresponding to a firing rate of $29.3\ \mathrm{Hz}$, which reflects entrainment to the external-field frequency.

Finally, we investigated the minimum gap-junction conductance required for the network to achieve full synchrony in the presence of an external electric field. We denote this quantity by g_{min} and define full synchrony as the condition $M \geq 0.99$. Figure 6 shows the variation of g_{min} across the V_{EF}-f_{EF} plane.

In the absence of an external electric field, we find $g_{\mathrm{min}} = 1.03\ \mathrm{mS/cm^2}$. When the field is applied, g_{min} covers a broad range between 0.29 and $1.45\ \mathrm{mS/cm^2}$, indicating that the electric field may facilitate, hinder, or exert no significant influence on the achievement of complete synchrony, depending on its parameters. Generally, the smallest values of g_{min} appear at high field amplitudes and high frequencies, although some minimums are observed near $(V_{\mathrm{EF}}, f_{\mathrm{EF}}) \approx (2.4\ \mathrm{mV}, 49\ \mathrm{Hz})$.

For medium-range amplitudes and high frequencies, g_{min} increases, indicating that stronger electrical coupling is required for complete synchrony. Overall, the dependence of g_{min} on the amplitude and frequency of the external electric field is highly irregular and nonlinear, reflecting the complex interplay between field-induced forcing and intrinsic network dynamics.

Figure 6: *Minimum gap-junction conductance g_{min}, shown by the color bar, required for a network of three all-to-all coupled HH neurons to achieve full synchrony $(M \geq 0.99)$ across the V_{EF}-f_{EF} plane. The injected currents are $I_{\mathrm{inj},1} = 6.15\ \mu\mathrm{A/cm^2}$, $I_{\mathrm{inj},2} = 10.5\ \mu\mathrm{A/cm^2}$, and $I_{\mathrm{inj},3} = 22.4\ \mu\mathrm{A/cm^2}$.*

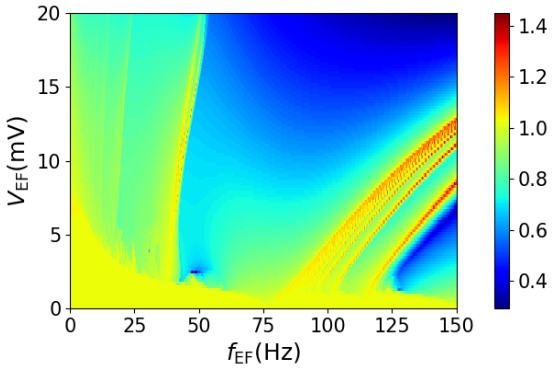

4. Conclusion

In this study, we examined the influence of an ELF sinusoidal external electric field on the collective dynamics of a three-neuron HH network with heterogeneous intrinsic firing frequencies. Our results reveal a rich set of behaviors arising from the nonlinear interplay among the external field, intrinsic neuronal properties, and gap-junction coupling.

Unlike previous two-neuron studies which only reported field-induced synchronization within a limited parameter range (*Wang et al., 2009; Che et al., 2009; Wang et al., 2007; Nkomidio et al., 2022*), our three-neuron investigation systematically explores a wide region of field frequencies and amplitudes. We found that the external electric field can not only enhance but also reduce or leave unchanged both the synchrony and the firing rate of the network. The particular outcome depends sensitively on the field frequency, field amplitude, and the strength of electrical coupling. Across the parameter space, all three regimes—facilitation, degradation, and neutrality—can occur. Nevertheless, in general, high field frequencies and large amplitudes tend to promote higher synchrony.

In the absence of the external field, varying the gap-junction conductance does not produce hysteresis in the synchrony measure. In contrast, the presence of the field can induce explosive transitions, some of which are accompanied by hysteresis loops, although such loops appear only rarely and with very narrow width.

Finally, our analysis of the minimum gap-junction conductance required for full synchrony $(M \geq 0.99)$ shows that the external field may facilitate, make more difficult, or effectively leave unchanged the attainment of complete synchronization. This dependence is highly irregular across the V_{EF}-f_{EF} parameter space, underscoring the complex and nonlinear nature of field–neuron interactions.

Weak ELF fields act as a non-monotonic modulator of synchrony in small neural motifs. This study increases our knowledge on brain networks by showing that external fields can either enhance, reduce, or leave synchrony unchanged depending on field parameters—a context-dependent effect that matters because synchrony itself is essential for information transfer in neural systems (*Buzsaki & Draguhn, 2004*). The observation of explosive synchronization with narrow hysteresis offers a possible mechanism for abrupt state switching in neural assemblies. Furthermore, the high sensitivity of minimum gap-junction coupling to the external field implies that exogenous fields could alter effective connectivity without changing anatomical wiring. Together, these results bridge cellular-level field effects to emergent network dynamics, providing a deeper understanding of how weak electric fields may influence information processing and state transitions in brain networks.

Our simulations were performed on a three-neuron network, which can be viewed as a basic building block of larger neural networks. While findings such as the non-monotonic modulation of synchrony and explosive synchronization with hysteresis may qualitatively generalize to larger networks, larger networks can have different sizes and topologies, both of which can affect

synchrony. Therefore, definitive generalization cannot be claimed without further numerical and analytical investigations.

Overall, these findings deepen our understanding of how weak, time-varying electric fields influence the dynamics of electrically coupled neuronal networks and underscore the networks' sensitivity to subtle external perturbations.

References

Kama, H., Ying, L., Chun, Y., & Mingjun, G. (1997). The dynamic principle of interaction between weak electromagnetic fields and living system--Interference of electromagnetic waves in dynamic metabolism. *Chinese Journal of Medical Physics*, *14*(4), 205-207.

Peterchev, A. V., Wagner, T. A., Miranda, P. C., Nitsche, M. A., Paulus, W., Lisanby, S. H., ... & Bikson, M. (2012). Fundamentals of transcranial electric and magnetic stimulation dose: definition, selection, and reporting practices. *Brain stimulation*, *5*(4), 435-453. https://doi.org/10.1016/j.brs.2011.10.001

Rubin, J. E., & Terman, D. (2004). High frequency stimulation of the subthalamic nucleus eliminates pathological thalamic rhythmicity in a computational model. *Journal of computational neuroscience*, *16*(3), 211-235. https://doi.org/10.1023/B:JCNS.0000025686.47117.67

Hariz, M., & Blomstedt, P. (2022). Deep brain stimulation for Parkinson's disease. *Journal of internal medicine*, *292*(5), 764-778. https://doi.org/10.1111/joim.13541

Krack, P., Batir, A., Van Blercom, N., Chabardes, S., Fraix, V., Ardouin, C., ... & Pollak, P. (2003). Five-year follow-up of bilateral stimulation of the subthalamic nucleus in advanced Parkinson's disease. *New England Journal of Medicine*, *349*(20), 1925-1934. https://doi.org/10.1056/NEJMoa035275

Toda, H., Hamani, C., & Lozano, A. (2004). Deep brain stimulation in the treatment of dyskinesia and dystonia. *Neurosurgical focus*, *17*(1), 9-13. https://doi.org/10.3171/foc.2004.17.1.2

Hale, A. T., Monsour, M. A., Rolston, J. D., Naftel, R. P., & Englot, D. J. (2020). Deep brain stimulation in pediatric dystonia: a systematic review. *Neurosurgical review*, *43*(3), 873-880. https://doi.org/10.1007/s10143-018-1047-9

Wagner, T., Valero-Cabre, A., & Pascual-Leone, A. (2007). Noninvasive human brain stimulation. *Annu. Rev. Biomed. Eng.*, *9*(1), 527-565. https://doi.org/10.1146/annurev.bioeng.9.061206.133100

Walsh, V., & Cowey, A. (2000). Transcranial magnetic stimulation and cognitive neuroscience. *Nature Reviews Neuroscience*, *1*(1), 73-80. https://doi.org/10.1038/35036239

Walton, D., Spencer, D. C., Nevitt, S. J., & Michael, B. D. (2021). Transcranial magnetic stimulation for the treatment of epilepsy. *Cochrane Database of Systematic Reviews*, (4). https://doi.org/10.1002/14651858.CD011025.pub3

Somaa, F. A., de Graaf, T. A., & Sack, A. T. (2022). Transcranial magnetic stimulation in the treatment of neurological diseases. *Frontiers in neurology*, *13*, 793253. https://doi.org/10.3389/fneur.2022.793253

Klimesch, W., Sauseng, P., & Gerloff, C. (2003). Enhancing cognitive performance with repetitive transcranial magnetic stimulation at human individual alpha frequency. *European Journal of Neuroscience*, *17*(5), 1129-1133. https://doi.org/10.1046/j.1460-9568.2003.02517.x

Mellon, N., Robbins, B., van Bruggen, R., & Zhang, Y. (2024). A systematic review and meta-analysis of the preclinical and clinical results of low-field magnetic stimulation in cognitive disorders. *Reviews in the Neurosciences*, *35*(6), 619-625. https://doi.org/10.1515/revneuro-2024-0023

Mert, T. (2017). Pulsed magnetic field treatment as antineuropathic pain therapy. *Reviews in the Neurosciences*, *28*(7), 751-758. https://doi.org/10.1515/revneuro-2017-0003

Roth, B. J., & Basser, P. J. (2002). A model of the stimulation of a nerve fiber by electromagnetic induction. *IEEE Transactions on Biomedical Engineering*, *37*(6), 588-597. https://doi.org/10.1109/10.55662

Lv, M., & Ma, J. (2016). Multiple modes of electrical activities in a new neuron model under electromagnetic radiation. *Neurocomputing*, *205*, 375-381. https://doi.org/10.1016/j.neucom.2016.05.004

Giannì, M., Liberti, M., Apollonio, F., & D'Inzeo, G. (2006). Modeling electromagnetic fields detectability in a HH-like neuronal system: stochastic resonance and window behavior. *Biological Cybernetics*, *94*(2), 118-127. https://doi.org/10.1007/s00422-005-0029-5

Li, J., Liu, S., Liu, W., Yu, Y., & Wu, Y. (2016). Suppression of firing activities in neuron and neurons of network induced by electromagnetic radiation. *Nonlinear Dynamics*, *83*(1), 801-810. https://doi.org/10.1007/s11071-015-2368-7

Doi, S., Nabetani, S., & Kumagai, S. (2001). Complex nonlinear dynamics of the Hodgkin–Huxley equations induced by time scale changes. *Biological cybernetics*, *85*(1), 51-64. https://doi.org/10.1007/PL00007996

Gu, H., Yang, M., Li, L., Liu, Z., & Ren, W. (2003). Noise induced multi-mode neural firings in a period adding bifurcation scenario. *International Journal of Modern Physics B*, *17*(22n24), 4195-4200. https://doi.org/10.1142/S0217979203022179

Wu-Yin, J., Jian-Xue, X., Ying, W., & Ling, H. (2004). An alternating periodic–chaotic ISI sequence of HH neuron under external sinusoidal stimulus. *Chinese Physics*, *13*(3), 335. https://doi.org/10.1088/1009-1963/13/3/012

Smeal, R. M., Ermentrout, G. B., & White, J. A. (2010). Phase-response curves and synchronized neural networks. *Philosophical Transactions of the Royal Society B: Biological Sciences*, *365*(1551), 2407-2422. https://doi.org/10.1098/rstb.2009.0292

Hodgkin, A. L., & Huxley, A. F. (1952). A quantitative description of membrane current and its

application to conduction and excitation in nerve. *The Journal of physiology*, *117*(4), 500. https://doi.org/10.1113/jphysiol.1952.sp004764

Izhikevich, E. M. (2004). Which model to use for cortical spiking neurons?. *IEEE transactions on neural networks*, *15*(5), 1063-1070. https://doi.org/10.1109/TNN.2004.832719

Morris, C., & Lecar, H. (1981). Voltage oscillations in the barnacle giant muscle fiber. *Biophysical journal*, *35*(1), 193-213. https://doi.org/10.1016/S0006-3495(81)84782-0

Rinzel, J., & Ermentrout, G. B. (1998). Analysis of neural excitability and oscillations. *Methods in neuronal modeling*, *2*, 251-292.

Saby, J. N., & Marshall, P. J. (2012). The utility of EEG band power analysis in the study of infancy and early childhood. *Developmental neuropsychology*, *37*(3), 253-273. https://doi.org/10.1080/87565641.2011.614663

Tian, H., Zhu, H., Gao, C., Shi, M., Yang, D., Jin, M., ... & Sui, X. (2023). System-level biological effects of extremely low-frequency electromagnetic fields: an in vivo experimental review. *Frontiers in Neuroscience*, *17*, 1247021. https://doi.org/10.3389/fnins.2023.1247021

Che, Y. Q., Wang, J., Si, W. J., & Fei, X. Y. (2009). Phase-locking and chaos in a silent Hodgkin–Huxley neuron exposed to sinusoidal electric field. *Chaos, Solitons & Fractals*, *39*(1), 454-462. https://doi.org/10.1016/j.chaos.2007.03.008

Han, C., Wang, J., & Deng, B. (2009). Fire patterns of modified HH neuron under external sinusoidal ELF stimulus. *Chaos, Solitons & Fractals*, *41*(4), 2045-2054. https://doi.org/10.1016/j.chaos.2008.08.011

Yi, G. S., Wang, J., Han, C. X., Deng, B., & Wei, X. L. (2012). Spiking patterns of a minimal neuron to ELF sinusoidal electric field. *Applied Mathematical Modelling*, *36*(8), 3673-3684. https://doi.org/10.1016/j.apm.2011.11.012

Nkomidio, A. M., Ngamga, E. K., Nbendjo, B. R. N., Kurths, J., & Marwan, N. (2022). Recurrence-based synchronization analysis of weakly coupled bursting neurons under external ELF fields. *Entropy*, *24*(2), 235. https://doi.org/10.3390/e24020235

Yi, G., Wang, J., Wei, X., Deng, B., Li, H., & Han, C. (2014). Dynamic analysis of Hodgkin's three classes of neurons exposed to extremely low-frequency sinusoidal induced electric field. *Applied Mathematics and Computation*, *231*, 100-110. https://doi.org/10.1016/j.amc.2013.12.181

Gholampour, M., Mahdavi, E., & Amirzadeh, M. (2026). Modulated nonlinear dynamics and mode-locking in silent Hodgkin–Huxley neurons exposed to extremely low-frequency electric field. *Journal of the Korean Physical Society*, 1-13. https://doi.org/10.1007/s40042-026-01597-6

Wang, J., Zhang, H., & Tsang, K. M. (2003, September). Hopf bifurcation in the Hodgkin-Huxley model exposed to ELF electrical field. In *Proceedings of the 25th Annual International Conference of the IEEE Engineering in Medicine and Biology Society (IEEE Cat. No.*

03CH37439) (Vol. 3, pp. 2323-2326). IEEE. https://doi.org/10.1109/IEMBS.2003.1280381

Jiang, W., Yanqiu, C., Xiangyang, F., & Li, L. (2005). Multi-parameter Hopf-bifurcation in Hodgkin–Huxley model exposed to ELF external electric field. *Chaos, Solitons & Fractals*, *26*(4), 1221-1229. https://doi.org/10.1016/j.chaos.2005.02.042

Wang, J., Che, Y. Q., Zhou, S. S., & Deng, B. (2009). Unidirectional synchronization of Hodgkin–Huxley neurons exposed to ELF electric field. *Chaos, Solitons & Fractals*, *39*(3), 1335-1345. https://doi.org/10.1016/j.chaos.2007.05.016

Che, Y. Q., Wang, J., Zhou, S. S., & Deng, B. (2009). Synchronization control of Hodgkin–Huxley neurons exposed to ELF electric field. *Chaos, Solitons & Fractals*, *40*(4), 1588-1598. https://doi.org/10.1016/j.chaos.2007.09.046

Wang, J., Zhang, T., & Che, Y. (2007). Chaos control and synchronization of two neurons exposed to ELF external electric field. *Chaos, Solitons & Fractals*, *34*(3), 839-850. https://doi.org/10.1016/j.chaos.2006.03.098

Yang, H., Wang, H., Guo, L., & Xu, G. (2022). Dynamic responses of neurons in different states under magnetic field stimulation. *Journal of Computational Neuroscience*, *50*(1), 109-120. https://doi.org/10.1007/s10827-021-00796-3

Yi, G., Wang, J., Wei, X., Deng, B., Tsang, K. M., Chan, W. L., & Han, C. (2014). Effects of extremely low-frequency magnetic fields on the response of a conductance-based neuron model. *International journal of neural systems*, *24*(01), 1450007. https://doi.org/10.1142/S0129065714500075

Buzsaki, G., & Draguhn, A. (2004). Neuronal oscillations in cortical networks. *science*, *304*(5679), 1926-1929. https://doi.org/10.1126/science.1099745

Attwell, D. (2003). Interaction of low frequency electric fields with the nervous system: the retina as a model system. *Radiation protection dosimetry*, *106*(4), 341-348. https://doi.org/10.1093/oxfordjournals.rpd.a006370

Bédard, C., Kröger, H., & Destexhe, A. (2006). Model of low-pass filtering of local field potentials in brain tissue. *Physical Review E—Statistical, Nonlinear, and Soft Matter Physics*, *73*(5), 051911. https://doi.org/10.1103/PhysRevE.73.051911

Börgers, C. (2017). *An introduction to modeling neuronal dynamics* (Vol. 66). Berlin: Springer. https://doi.org/10.1007/978-3-319-51171-9